

Thermodynamics and thin film deposition of MgB₂ superconductors

This content has been downloaded from IOPscience. Please scroll down to see the full text.

2002 Supercond. Sci. Technol. 15 451

(<http://iopscience.iop.org/0953-2048/15/3/333>)

View [the table of contents for this issue](#), or go to the [journal homepage](#) for more

Download details:

IP Address: 128.84.143.26

This content was downloaded on 16/06/2015 at 18:07

Please note that [terms and conditions apply](#).

Thermodynamics and thin film deposition of MgB₂ superconductors

X X Xi¹, X H Zeng¹, A Soukiassian¹, J Jones¹, J Hotchkiss¹, Yu Zhong², C O Brubaker², Zi-Kui Liu², J Lettieri², D G Schlom², Y F Hu¹, E Wertz¹, Qi Li¹, W Tian³, H P Sun³ and X Q Pan³

¹ Department of Physics, The Pennsylvania State University, University Park, PA 16802, USA

² Department of Materials Science and Engineering, The Pennsylvania State University, University Park, PA 16802, USA

³ Department of Materials Science and Engineering, The University of Michigan, Ann Arbor, MI 48109, USA

Received 20 August 2001

Published 12 February 2002

Online at stacks.iop.org/SUST/15/451

Abstract

The recently discovered superconductor MgB₂ with T_c at 39 K has great potential in superconducting microelectronics. Thermodynamics studies with the calculation of phase diagrams (CALPHAD) modelling technique show that due to the high volatility of Mg, MgB₂ is only thermodynamically stable under fairly high Mg overpressures for likely *in situ* growth temperatures. This provides a helpful insight into the appropriate processing conditions for MgB₂ thin films, including the identification of the pressure–temperature region for adsorption-controlled growth. The initial MgB₂ thin films were made by pulsed laser deposition followed by *in situ* annealing. The cross-sectional transmission electron microscopy reveals a nanocrystalline mixture of textured MgO and MgB₂ with very small grain sizes. A zero-resistance transition temperature of 34 K and a zero-field critical current density of 1.3×10^6 A cm⁻² were obtained. The qualities of these films are limited by the thermodynamic stability conditions, which favour deposition techniques that can maintain a high flux of Mg.

1. Introduction

The recent discovery of superconductivity in MgB₂ at 39 K has generated great interest [1, 2]. MgB₂ has the highest T_c known for non-oxide compounds. It has been shown that MgB₂ is a phonon-mediated BCS superconductor [3] with an energy gap of 5.2 meV at 4.2 K [4] and a coherence length of 50 Å [5]. Its grain boundaries do not have a large detrimental effect on the superconducting current transport [6, 7]. These properties hold tremendous promise for current-carrying large-scale applications in wires and tapes. They also suggest that Josephson junctions of MgB₂ may be much easier to fabricate than those made from the high temperature superconductors, which have much shorter coherence lengths. Such junctions could have the performance of conventional superconductor junctions, such as Nb and NbN, but operate at a much higher temperature.

A MgB₂ film processing technique compatible with multilayer depositions is needed for Josephson junction

applications. Currently, two main types of deposition processes have been used, both involving annealing of films deposited at low temperatures. The first type employs *ex situ* annealing of low-temperature deposited B or Mg + B films at 900 °C in Mg vapour. The resultant films exhibit bulk-like $T_{c0} \sim 39$ K [8–10] and extremely high critical current density ($\sim 10^7$ A cm⁻² at low temperatures) [11, 12]. However, the high-temperature *ex situ* annealing is unlikely to be compatible with multilayer device fabrications. The second type uses an *in situ* two-step process. Thin films or multilayers of Mg + B or Mg + MgB₂ are deposited at low temperatures, and then annealed *in situ* in the deposition chamber at about 600 °C [8, 13–15]. This process is potentially more compatible with junction fabrications, however the superconducting properties in such films are poorer than in the *ex situ* annealed films.

Due to the high volatility of Mg, the fabrication of MgB₂ thin films by *in situ* deposition is expected to be difficult. It has been demonstrated for numerous materials containing a volatile constituent that an understanding of

the thermodynamics of the system can help identify the appropriate growth regime for these materials [16–20]. In this paper, we discuss a thermodynamic analysis of the Mg–B system, which shows that the MgB₂ phase is thermodynamically stable only under high Mg partial pressures. The result not only provides helpful insights into appropriate processing conditions for *in situ* deposition of MgB₂ thin films, but also shows the limitation of the deposition technique involving *in situ* annealing. The result of MgB₂ thin films made by an *in situ* process using pulsed laser deposition (PLD) is then presented. It shows that the superconducting properties of these films are weakened by the small MgB₂ grain size of less than 50 Å.

2. Thermodynamics of the Mg–B system

Although MgB₂ has been known and structurally characterized since the mid 1950s [21], no detailed thermodynamics information is available in the literature [22]. Our approach of the thermodynamic analysis is the calculation of phase diagrams (CALPHAD), a thermodynamic modelling technique using a computerized optimization procedure. In the CALPHAD approach, the Gibbs energies of individual phases in a system are constructed with models primarily based on the crystal structures of the phases [23]. For pure elements, the most commonly used model is that suggested by the Scientific Group Thermodata Europe (SGTE). The SGTE data used here are compiled by Dinsdale [24]. Using the experimentally measured enthalpy of formation and estimated decomposition temperatures, the Gibbs energy of each phase is evaluated with the Thermo-Calc program [25]. The phase equilibria are then calculated.

In the Mg–B system, there are three intermediate compounds, MgB₂, MgB₄ and MgB₇, in addition to gas and the solution phases, i.e. liquid, *hcp* magnesium and β -rhombohedral boron [26]. The Gibbs energy of the gas phase assuming ideal mixing is

$$G_m = \sum y_i^\circ G_i + RT \sum y_i \ln y_i \quad (1)$$

where y_i and $^\circ G_i$ are the mole fraction and Gibbs energy of species i in the gas phase. The Gibbs energy of the solution phases treated as substitutional solutions is

$$G_m^\Phi = x_Mg^\circ G_Mg^\Phi + x_B^\circ G_B^\Phi + RT(x_Mg \ln x_Mg + x_B \ln x_B) \quad (2)$$

where $^\circ G_i^\Phi$ is the molar Gibbs energy of the pure element with the structure Φ from [24]. The Gibbs energies for the intermediate compounds are written using the two-sublattice model as

$$G_m^{MgB_x} = ^\circ G_{Mg}^{hcp} + x^\circ G_B^{\beta-rho} + (1+x)(a^{MgB_x} + b^{MgB_x} T) \quad (3)$$

where $^\circ G_{Mg}^{hcp}$ and $^\circ G_B^{\beta-rho}$ are the molar Gibbs energies of the *hcp* Mg and the β -rhombohedral B, respectively, a^{MgB_x} and b^{MgB_x} are the parameters to be determined, and $\Delta G_m^{MgB_x} = a^{MgB_x} + b^{MgB_x} T$ represents the Gibbs energy of formation of the compound MgB _{x} with x being 2, 4 and 7, respectively, expressed in per mole of atoms.

Using the aforementioned procedure, the Gibbs energies of formation are obtained for the three compounds:

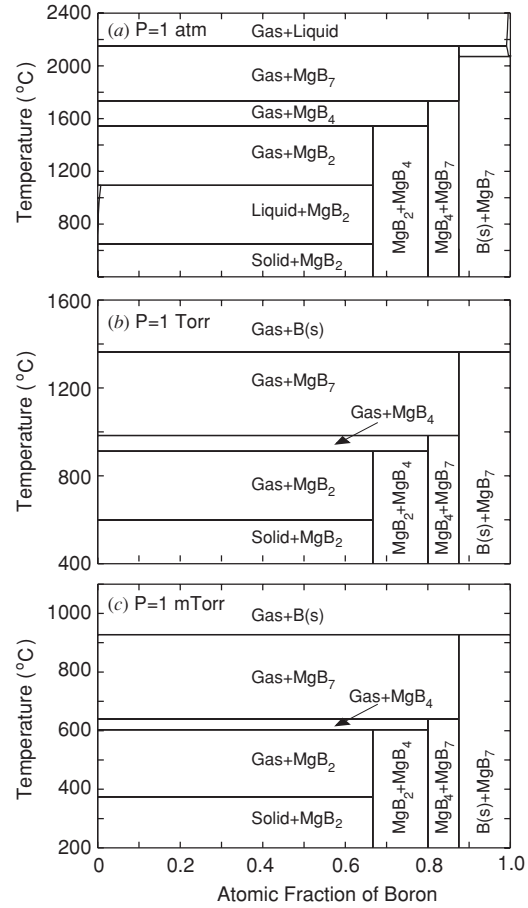


Figure 1. The temperature-composition phase diagrams of the Mg–B system under the pressures of (a) 1 atm, (b) 1 Torr and (c) 1 mTorr.

$\Delta G_m^{MgB_2} = -17121 - 3.815T$, $\Delta G_m^{MgB_4} = -14441 - 2.458T$ and $\Delta G_m^{MgB_7} = -13022 - 0.872T$. From these results, binary phase diagrams can be calculated. In figure 1 the calculated temperature-composition phase diagrams for the Mg–B system at (a) 1 atm, (b) 1 Torr and (c) 1 mTorr are plotted. The result for 1 atm pressure is consistent with the published Mg–B phase diagram [22], which confirms the powerful capability of the CALPHAD technique. Above 1545 °C MgB₂ decomposes into a mixture of MgB₄ and Mg vapour. When the pressure is reduced to 1 Torr, the phase diagram changes dramatically. Since the pressure is lower than the triple-point pressure of Mg (650 °C, 2.93 Torr), the liquid phase of Mg disappears completely. The decomposition temperature of MgB₂ decreases to 912 °C. This temperature decreases further to 603 °C at a pressure of 1 mTorr. It is evident that Mg overpressure has a significant influence on the decomposition temperature of MgB₂, which can be very low, thus severely limiting the thin film deposition temperature.

The kinetics of crystal growth require that an *in situ* film deposition process takes place at sufficiently high temperatures. The optimum temperature for epitaxial growth is typically about one half of the melting temperature, T_m (in Kelvin), although the minimum temperature can be much lower [27]. For example, the minimum epitaxial growth temperature for metals is about $T_m/8$ [28]. Thermodynamic

calculation shows that MgB₂ melts congruently at 2430 °C (~2700 K) with an equilibrium vapour pressure exceeding 49000 Torr. Therefore, the optimum temperature for the deposition of epitaxial MgB₂ films is around ~1080 °C (1350 K). For MgB₂ to be stable at 1080 °C, a Mg partial pressure of at least 11 Torr is required. Converting the Mg partial pressure to Mg flux, F , from the deposition source using the formula $F = P/\sqrt{2\pi mk_B T}$, where m is the mass of Mg atom [29, 30], 11 Torr is equivalent to an incident Mg flux of 2×10^{21} Mg atoms/(cm² s), or a Mg deposition rate of 0.5 mm s⁻¹ if all the Mg atoms stick and form a Mg layer with bulk density. This is impossible for most thin film deposition techniques.

Figure 1, however, illustrates the automatic composition control benefit that accompanies adsorption-controlled growth as is extensively used for III–V and II–VI compound semiconductors [31]. As long as the Mg:B ratio is above the 1:2 stoichiometry, any amount of extra Mg above this stoichiometric amount will vaporize and the desired MgB₂ phase will result. The most critical requirement for controlling the stoichiometry is thus to avoid insufficient Mg supply, which will lead to MgB₄, MgB₇ or solid B phases.

From a thermodynamic perspective, deposition of a single-phase MgB₂ film becomes easy when the growth conditions (substrate temperature and Mg overpressure) fall within a window where the thermodynamically stable phases are the desired MgB₂ phase and gas phases. Within this growth window MgB₂ does not decompose and excess Mg does not condense on the MgB₂ surface, thus the formation of single-phase MgB₂ is adsorption controlled and automatic. This window (the ‘Gas + MgB₂’ region) is best illustrated by the pressure–temperature phase diagram shown in figure 2. For a given deposition temperature, one can find the Mg partial pressure range to keep the MgB₂ phase thermodynamically stable. As shown in the figure, this range extends over about three orders of magnitude. The boundaries of the growth window can be approximately expressed by the following equations: $\log(P) = -7561/T + 8.673$ (the upper boundary with solid Mg) and $\log(P) = -10142/T + 8.562$ (the lower boundary with MgB₄), where P is in Torr and T in Kelvin.

While the applicability of equilibrium thermodynamics to thin film growth has been established for many material systems, the non-equilibrium nature of specific deposition techniques can be quite important. For MgB₂, a recent study has revealed a significant kinetic barrier to the thermal decomposition of MgB₂ [32]. This opens the possibility of using non-equilibrium routes to drive the formation reaction of MgB₂ to mitigate by as much as a factor of 10⁻³ the high Mg pressures described in this paper.

The implications of the thermodynamic analysis to the *in situ* MgB₂ film deposition can be demonstrated by examining the necessary Mg overpressures for several possible deposition conditions. As discussed above, the optimum epitaxial growth temperature is ~1080 °C for MgB₂, which requires a Mg flux of 2×10^{21} Mg atoms/(cm² s) or a Mg deposition rate of 0.5 mm s⁻¹. The lower bound for epitaxial growth is unknown. For metals it is about $T_m/8$ [28], which would be 50 °C for MgB₂. However, there has been no observation of MgB₂ epitaxy for a deposition temperature lower than 400 °C. From the phase diagram in

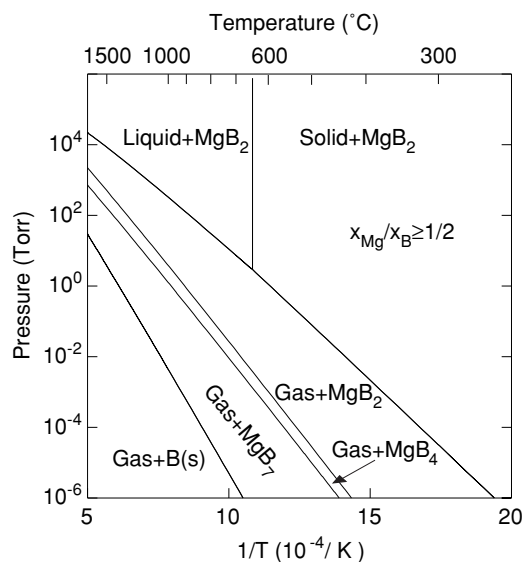


Figure 2. The pressure–temperature phase diagram for the Mg:B atomic ratio $x_{\text{Mg}}/x_{\text{B}} \geq 1/2$. The region of ‘gas + MgB₂’ represents the thermodynamic stability window for the deposition of MgB₂ thin films.

figure 2, a deposition temperature of 850 °C corresponds to a Mg overpressure of 340 mTorr, or a Mg flux of 6×10^{19} Mg atoms/(cm² s) or a Mg deposition rate of 15 μm s⁻¹. For 600 °C, the necessary Mg overpressure is 0.9 mTorr, which corresponds to a Mg flux of 2×10^{17} Mg atoms/(cm² s) or a Mg growth rate of 500 Å s⁻¹. Clearly, these conditions favour deposition techniques that can maintain a high Mg overpressure during the deposition. This is further complicated by the oxygen contamination during the deposition in non-UHV systems. The Mg flux reacts with residual oxygen in the background, which effectively reduces the Mg overpressure thus pushing the system to the thermodynamically unstable region.

3. Nanocrystalline MgB₂ thin films by an *in situ* annealing process

Before an *in situ* MgB₂ thin film deposition technique that satisfies the thermodynamic stability conditions is developed, techniques involving post-deposition annealing are being investigated. We have used PLD with an *in situ* annealing procedure similar to those described by Blank *et al* [13], Christen *et al* [14] and Shinde *et al* [8], which is potentially more compatible with junction fabrications than the *ex situ* annealing process. The early reports from various groups on *in situ* MgB₂ thin films show lower T_{c0} around or below 25 K [8, 13–15]. Our result shows a much higher T_{c0} of 34 K. From the structural analysis, we find that our films are nanocrystalline and the small MgB₂ size limits their superconducting properties.

The MgB₂ films were deposited on (0001) Al₂O₃ substrates from targets prepared by pressing Mg powder with MgB₂ powder at room temperature. The Mg:MgB₂ molar ratio was varied between 4:1 and 2:1. The films were deposited at 250–300 °C in an Ar atmosphere (99.999% gas purity) of 120 mTorr. The background vacuum was in the low to mid

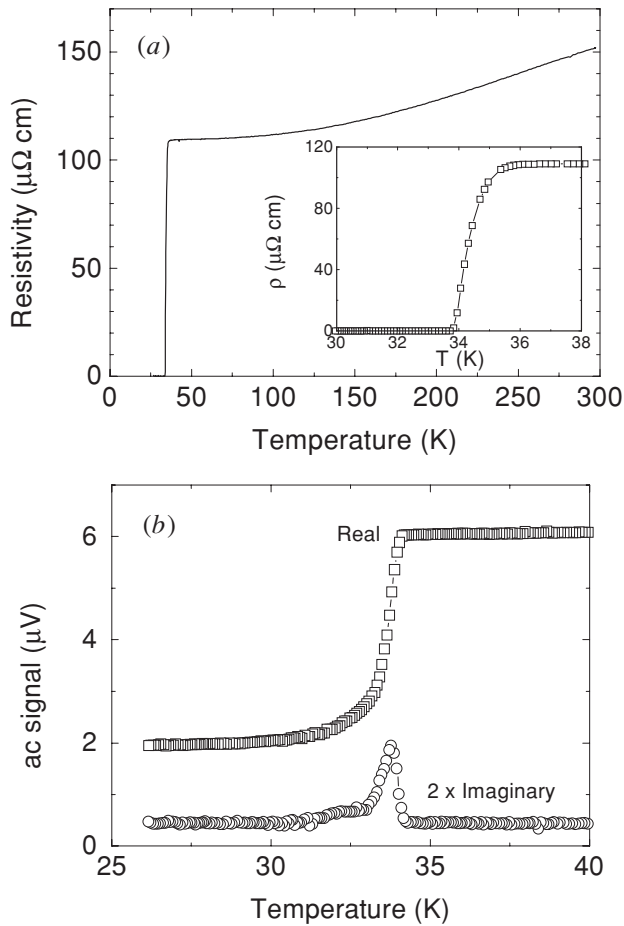


Figure 3. (a) Resistivity versus temperature curve for a 4000 Å thick MgB₂ film. (b) The ac susceptibility of the same film.

10^{-7} Torr range. The energy density of the laser beam was 5 J cm^{-2} and the repetition rate was 5 Hz. The deposited films were then heated at a rate of $40 \text{ }^\circ\text{C min}^{-1}$ to $630 \text{ }^\circ\text{C}$ and held there for 10 min. The atmosphere during the heating and annealing was the same as during the deposition. After the *in situ* annealing, the films were cooled to room temperature in ~ 20 Torr Ar.

The film deposited at $250\text{--}300 \text{ }^\circ\text{C}$ was a likely mixture of Mg and amorphous MgB₂ or B. Several processes are involved in the *in situ* annealing: Mg evaporation, MgB₂ phase formation, which is determined by the thermodynamics [33] and forward kinetics [32], nucleation and growth of crystallites, and MgB₂ decomposition, which is determined by the thermodynamics [33] and a kinetic barrier [32]. High quality films are constrained by the balance of these processes, and a careful adjustment of the heating and annealing parameters such as temperature and duration is necessary.

In figure 3(a) we plot the resistivity versus temperature curve for a 4000 Å thick MgB₂ film. It shows a metallic behaviour with a residual resistance ratio, $\text{RRR} = R(300 \text{ K})/R(40 \text{ K})$, of 1.4 and the resistivity at room temperature is $\sim 150 \mu\Omega \text{ cm}$. Compared to high-density bulk samples, where $\text{RRR} = 25.3$ and $\rho(300 \text{ K}) = 9.6 \mu\Omega \text{ cm}$ [34], the residual resistance ratio of the MgB₂ film is much smaller and the resistivity much higher. This is likely to be due to the small grain sizes and existence of MgO in the film since precipitates

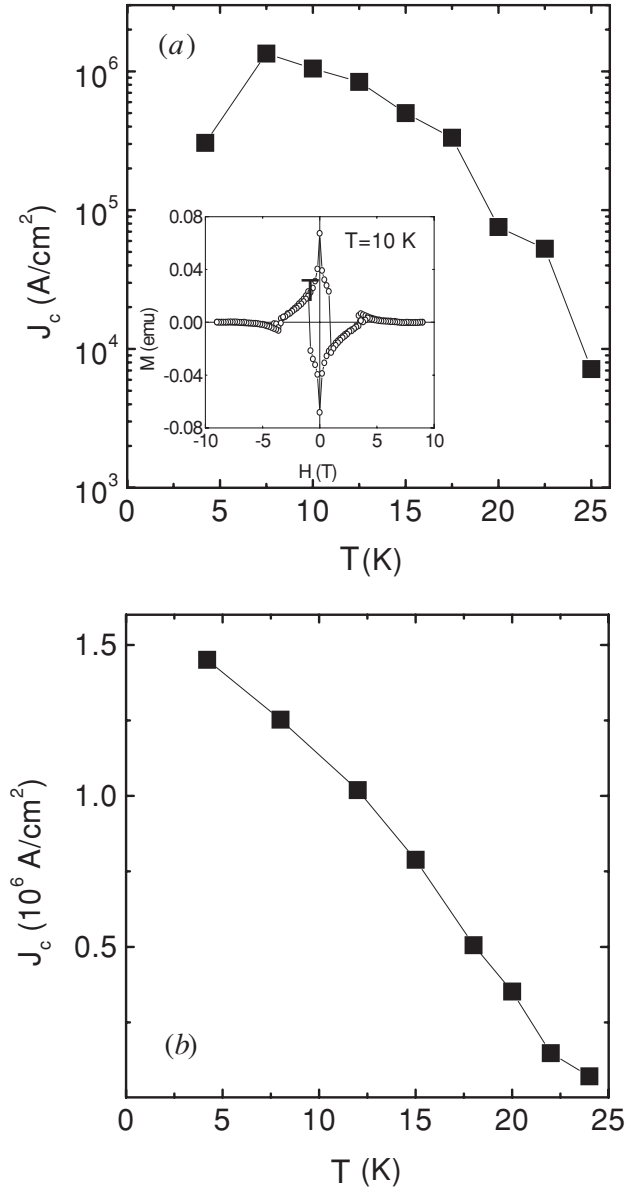


Figure 4. The temperature dependence of the zero-field J_c of a 4000 Å thick MgB₂ film. The inset shows the M - H loop at $T = 10 \text{ K}$.

of MgO at the grain boundaries will act as series-connected resistors to the MgB₂ grains. The superconducting transition temperature of the film, characterized by the zero resistance temperatures, is 34 K. The superconducting transition is further characterized by the ac susceptibility, the result of which is shown in figure 3(b). The transition is relatively sharp with a full width at the half maximum of the imaginary-part signal being $\sim 0.8 \text{ K}$.

The critical current densities of the MgB₂ films were determined using both the magnetization and transport methods. In figure 4(a), the temperature dependence of J_c is plotted for a 4000 Å thick MgB₂ film. A zero-field $J_c \sim 1.34 \times 10^6 \text{ A cm}^{-2}$ was obtained at 7.5 K. The M - H loop at 10 K for magnetic field $\mathbf{H} \perp$ film surface, which is $5 \text{ mm} \times 4 \text{ mm}$ in size, is shown in the inset. It shows a severe instability in flux pinning or flux jump, which causes the collapse of circulating critical current so that the magnetization

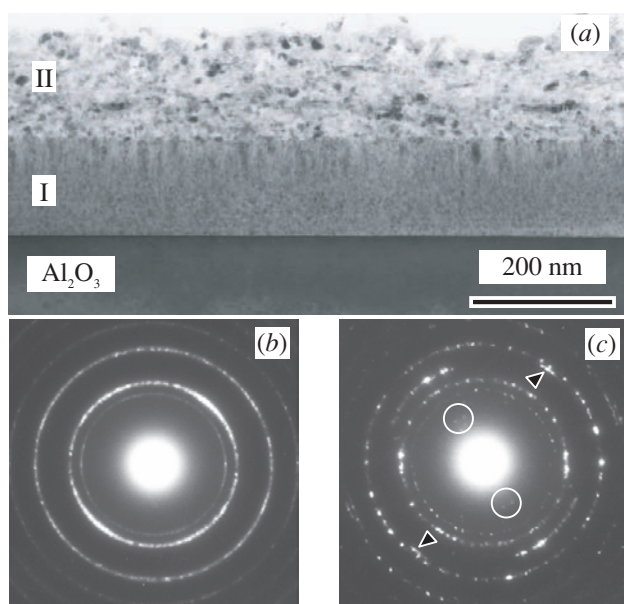


Figure 5. (a) Dark-field TEM image showing a cross-sectional view of a MgB₂ thin film with $T_c = 32$ K. Selected-area electron diffraction patterns from (b) region I and (c) region II.

curve returns to the reversible magnetization branch (in the II and IV quadrants). The actual closing of the hysteresis curve excluding the flux jump occurs at a field of ~ 8 T at low temperatures, suggesting an irreversibility field similar to that found in bulk MgB₂ [6]. The temperature dependence of the transport J_c is plotted in figure 4(b) for a 2500 Å thick MgB₂ film. A narrow bridge with a width of 7 μm was photolithographically patterned and the electrodes were formed by pressed indium. A criterion of 1 μV was used to determine the critical current. As shown in the figure, a J_c value of 1.4×10^6 A cm⁻² was obtained at low temperatures.

Compared to the early reports of *in situ* MgB₂ thin films [8, 13–15] where T_c is around or below 25 K, the T_c value shown here is much higher. The reason may be due to the different microstructures in these films. We have studied the structure of our films by both x-ray diffraction and cross-sectional transmission electron microscopy (TEM). In contrast to *ex situ* annealed MgB₂ films with bulk-like T_c of 39 K, which has a MgB₂ grain size of ~ 100 Å and clear x-ray diffraction peaks [11, 10], x-ray diffraction scans of our *in situ* annealed films revealed no discernable film peaks, indicating that the grain size was appreciably smaller. The correlation between the MgB₂ grain size and superconducting properties is further corroborated by the TEM results of two MgB₂ films of different T_c values.

The TEM result for a MgB₂ film with $T_c = 32$ K is shown in figure 5, and its R versus T curve is shown in figure 6. The dark-field image in figure 5(a) shows that the film consists of two layers with different contrast. Figure 5(b) is a selected-area electron diffraction pattern taken from region I near the film/substrate interface. By measuring the position and intensity distribution of the diffraction rings, it is determined that they all belong to the rock salt MgO phase. Figure 5(c) is a diffraction pattern taken from region II close to the film surface using the same size selected-area aperture as for figure 5(b). In addition to the diffraction rings corresponding to

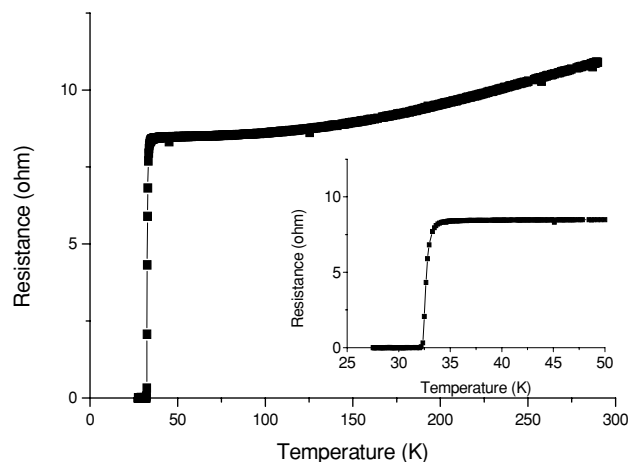


Figure 6. Resistance versus temperature curve for the film in figure 5.

the MgO phase, it also shows diffraction spots corresponding to the hexagonal MgB₂ phase. The diffraction spots indicated by the circles are due to the (001) planes, while those by the arrow heads arise from diffraction by the (110) planes of MgB₂. The (021) MgB₂ reflections are also detected. The discrete spots appear in figure 5(c) instead of nearly continuous rings in figure 5(b), indicating a larger grain size in region II. In both regions, the result indicates substantial oxygen contamination. The MgB₂ grain size in region I must be less than about 50 Å to account for the absence of MgB₂ rings or spots in figure 5(b).

The TEM result for a second MgB₂ film with $T_c = 21$ K is shown in figure 7, and its R versus T curve is shown in figure 8. From the dark-field image in figure 7(a) one can see that region I is thinner than that in the higher T_c film. As shown in figure 7(b), in both regions I and II, the MgB₂ diffraction patterns were absent. The absence of the MgB₂ patterns indicates that the MgB₂ grain size in this film is less than 50 Å. When the grain size is close to the coherence length of MgB₂, the superconducting properties will be affected. While the 900 °C annealing in the *ex situ* process provides enough thermal energy for crystallization and texturing, the lower temperature during the *in situ* annealing limits the extent of these processes. The reason that the T_c value reported here is much higher than those in the early reports of *in situ* MgB₂ thin films [8, 13–15] may be that the grain size in our film is larger due to the details of the processing conditions.

The results of both figures 5 and 7 show severe oxygen contamination in the films. The diffraction patterns from MgO dominate both images. A separate XPS measurement of two films with different T_c , 17 and 32 K, respectively, shows that there is no appreciable difference in the oxygen content between the two films, and the Mg:B:O atomic ratio is 1.0:1.1:1.2. The extent of the detrimental effects of oxygen contamination is not well understood, and Eom *et al* even suggest that it may help to enhance the flux pinning [11].

4. Conclusion

In order to realize the potential of MgB₂ in superconducting digital applications, epitaxial or polycrystalline film produced

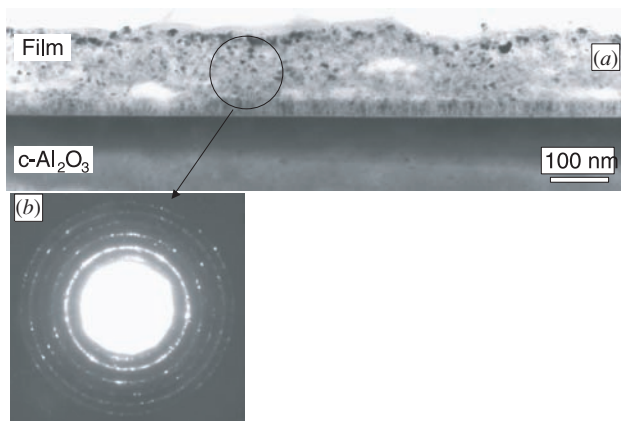


Figure 7. (a) Dark-field TEM image showing a cross-sectional view of a second MgB₂ thin film with $T_c = 21$ K. (b) Selected-area electron diffraction pattern.

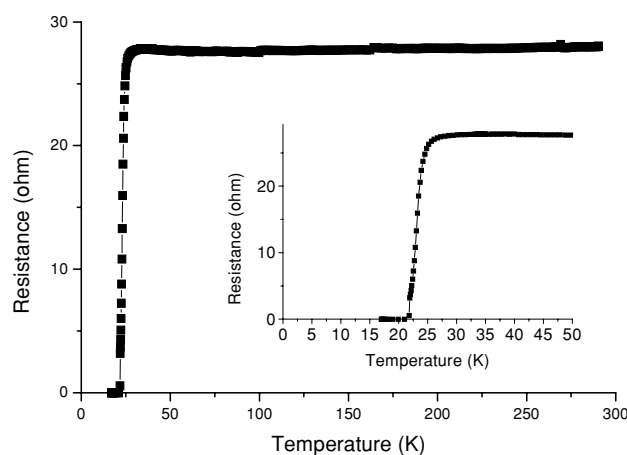


Figure 8. Resistance versus temperature curve for the film in figure 7.

by a processing technique compatible with multilayer depositions is needed. Using the CALPHAD technique we find that MgB₂ is thermodynamically stable only under fairly high to very high Mg partial pressures at the temperature range appropriate for epitaxial growth. Therefore, a large Mg flux must be delivered from the deposition source for *in situ* MgB₂ film deposition. This requirement favours deposition techniques that can maintain a large Mg flux over those where a large Mg flux is impractical. At present, no report of such deposition technique exists.

Lacking an *in situ* MgB₂ film deposition technique, we have deposited MgB₂ films by pulsed laser deposition using an *in situ* annealing process. The T_{c0} obtained is much higher than those previously reported *in situ* films and J_c is comparable to those of the polycrystalline bulk samples even though the grain size in the films is extremely small. Because this deposition process is more compatible with multilayer deposition, it is important to demonstrate that high T_{c0} and J_c can be obtained using this process. Our results are a step towards making the *in situ* annealing technique a viable candidate for MgB₂ Josephson junction technologies. However, because the formation and crystallization of the MgB₂ phase is constrained by the balance of several processes and by thermodynamic phase stability conditions and kinetics,

it is difficult to achieve films with large grain sizes. An *in situ* film deposition technique is much more desirable for the MgB₂ Josephson junction technologies.

Acknowledgments

This work is supported in part by ONR under grant no N00014-00-1-0294 (XXX), by NSF under grant nos DMR-9875405 and DMR-9871177 (XQP), DMR-9876266 and DMR-9972973 (QL), DMR-9983532 (ZKL), and by DOE through grant DE-FG02-97ER45638 (DGS).

References

- [1] Nagamatsu J, Nakagawa N, Muranaka T, Zenitani Y and Akimitsu J 2001 *Nature* **410** 63
- [2] Cava R J 2001 *Nature* **410** 23
- [3] Bud'ko S L, Lapertot G, Petrovic C, Cunningham C E, Anderson N and Canfield P C 2001 *Phys. Rev. Lett.* **86** 1877
- [4] Karapetrov G, Iavarone M, Kwok W K, Crabtree G W and Hinks D G 2001 *Phys. Rev. Lett.* **86** 4374
- [5] Finnemore D K, Ostenson J E, Bud'ko S L, Lapertot G and Canfield P C 2001 *Phys. Rev. Lett.* **86** 2420
- [6] Larbalestier D C *et al* 2001 *Nature* **410** 186
- [7] Bugoslavsky Y, Perkins G K, Qi X, Cohen L F and Caplin A D 2001 *Nature* **410** 563
- [8] Shinde S R, Ogale S B, Greene R L, Venkatesan T, Canfield P C, Bud'ko S, Lapertot G and Petrovic C 2001 *Appl. Phys. Lett.* **79** 227
- [9] Zhai H Y, Christen H M, Zhang L, Paranthaman M, Cantoni C, Sales B C, Fleming P H, Christen D K and Lowndes D H 2001 *Preprint cond-mat/0103618*
- [10] Kang W N, Kim H-J, Choi E-M, Jung C U and Lee S-I 2001 *Science* **292** 1521
- [11] Eom C B *et al* 2001 *Nature* **411** 558
- [12] Moon S H, Yun J H, Lee H N, Kye J I, Kim H G, Chung W and Oh B 2001 *Appl. Phys. Lett.* **79** 2429
- [13] Blank D H A, Hilgenkamp H, Brinkman A, Mijatovic D, Rijnders G and Rogalla H 2001 *Appl. Phys. Lett.* **79** 394
- [14] Christen H, Zhai H, Cantoni C, Paranthaman M, Sales B, Rouleau C, Norton D, Christen D and Lowndes D 2001 *Physica C* **353** 157
- [15] Grassano G, Ramadan W, Ferrando V, Bellingeri E, Marré D, Ferdeghini C, Grasso G, Putti M, Siri A S, Manfrinetti P, Palenzona A and Chincarini A 2001 *Supercond. Sci. Technol.* **14** 762–4
- [16] Heckingbottom R, Davies G and Prior K 1983 *Surf. Sci.* **132** 375
- [17] Seki H and Koukitu A 1986 *J. Cryst. Growth* **78** 342
- [18] Hammond R H and Bormann R 1989 *Physica C* **162** 703
- [19] Tsao J Y 1991 *J. Cryst. Growth* **110** 595
- [20] Theis C D, Yeh J, Schlom D G, Hawley M E and Brown G W 1998 *Thin Solid Films* **325** 107
- [21] Jones M and Marsh R 1954 *J. Amer. Chem. Soc.* **76** 1434
- [22] Massalski T (ed) 1990 *Binary Alloy Phase Diagrams* 2nd edn (Materials Park, OH: ASM International)
- [23] Saunders N and Miodownik A P 1998 *CALPHAD (Calculation of Phase Diagrams): A Comprehensive Guide* (Oxford: Pergamon)
- [24] Dinsdale A T 1991 *CALPHAD, Comput. Coupling Phase Diagr. Thermochem.* **15** 317
- [25] Jansson B, Jonsson B, Sundman B and Agren J 1993 *Thermochimica Acta* **214** 93
- [26] Nayeib-Hashemi A A and Clark J B 1988 *Phase Diagrams of Binary Magnesium Alloys* (Materials Park, OH: ASM International)
- [27] Yang M H and Flynn C P 1989 *Phys. Rev. Lett.* **62** 2476
- [28] Flynn C P 1988 *J. Phys. F* **18** L195

-
- [29] Loeb L B 1934 *The Kinetic Theory of Gases* (New York: McGraw-Hill) pp 19–106
- [30] Schlom D and Harris Jr J 1995 *Molecular Beam Epitaxy: Applications to Key Materials* ed R Farrow (Park Ridge: Noyes) p 505
- [31] Tsao J Y 1993 *Materials Fundamentals of Molecular Beam Epitaxy* (Boston: Academic)
- [32] Fan Z Y, Hinks D G, Newman N and Rowell J M 2001 *Appl. Phys. Lett.* **79** 87
- [33] Liu Z K, Schlom D G, Li Q and Xi X X 2001 *Appl. Phys. Lett.* **78** 3678
- [34] Canfield P C, Finnemore D K, Bud'ko S L, Ostenson J E, Lapertot G, Cunningham C E and Petrovic C 2001 *Phys. Rev. Lett.* **86** 2423